ACSNANO
www.acsnano.org

ARTICLE

# Acoustic Microcannons: Toward Advanced Microballistics

Fernando Soto,[†,∥] Aida Martin,[†,‡,∥] Stuart Ibsen,[†] Mukanth Vaidyanathan,[†] Victor Garcia-Gradilla,[†,§] Yair Levin,[†] Alberto Escarpa,[‡] Sadik C. Esener,[*,†] and Joseph Wang[*,†]

[†]Department of Nanoengineering, University of California San Diego, La Jolla, California 92093, United States
[‡]Department of Analytical Chemistry, University of Alcalá de Henares, E-28871 Madrid, Spain
[§]Center for Nanosciences and Nanotechnology, UNAM, Ensenada, 22800 Mexico

Supporting Information

**ABSTRACT:** **Acoustically triggered microcannons, capable of loading and firing nanobullets (Nbs), are presented as powerful microballistic tools. Hollow conically shaped microcannon structures have been synthesized electrochemically and fully loaded with nanobullets made of silica or fluorescent microspheres, and perfluorocarbon emulsions, embedded in a gel matrix stabilizer. Application of a focused ultrasound pulse leads to the spontaneous vaporization of the perfluorocarbon emulsions within the microcannon and results in the rapid ejection of the nanobullets. Such Nbs "firing" at remarkably high speeds (on the magnitude of meters per second) has been modeled theoretically and demonstrated experimentally. Arrays of microcannons anchored in a template membrane were used to demonstrate the efficient Nbs loading and the high penetration capabilities of the ejected Nbs in a tissue phantom gel. This acoustic-microcannon approach could be translated into advanced microscale ballistic tools, capable of efficient loading and firing of multiple cargoes, and offer improved accessibility to target locations and enhanced tissue penetration properties.**

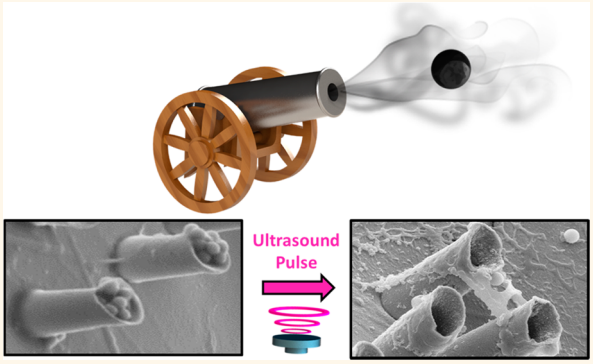


**KEYWORDS:** *microballistic, nanobullet, nanomachine, US-triggered, tissue penetration*

For over a decade, "magic bullets" that would drive drugs deep into diseased tissues have been a dream of biomedical researchers.[1,2] Such "magic bullet" vision has inspired and encouraged scientists to create efficient delivery devices toward the successful treatment of human diseases. Designing the right tool for efficient tissue penetration at small scales is essential for diverse applications in drug delivery and microsurgery applications. Novel micro/nanoscale ballistic tools could pave the way of deep tissue penetration on small scales, providing distinct advantages, due to their size and ability to reach places where catheters cannot. Powerful machinery, including ballistics, exists on the macroscopic scale to penetrate and cut through tissues. However, these large scale ballistic tools do not have analogous micro/nanoscale counterparts, hindering the ability to operate at this small scale and resulting in very limited tissue penetration. Traditional technology cannot be simply scaled down due to the dominating viscosity forces (over inertia forces) at smaller scales that affect both the movement and directionality.[3−6] Accordingly, small scale machinery tools need to be powered and actuated by fundamentally different approaches than macroscopic devices. New nanomachine strategies have been developed recently in this direction.[7−13] Such tiny machines are capable of performing diverse applications,[14−17] including some initial reports of microsurgery[18,19] and cell internalization.[20,21] However, obtaining a stable, controlled, powerful, and directed means for penetrating tissue and delivering payloads at these small scales remains a major technological challenge. Although bullet-shaped microstructure materials have been designed[22] and metallic microbullets are reported as therapeutic tools,[23,24] they do not offer penetration capabilities or motion, but rather they are only incubated with the target. Indeed, there are no earlier reports regarding the controlled firing of nanobullets from a microstructure.

To address this challenge and fill this technological gap, we demonstrate here the use of acoustically triggered microcannons (Mc), capable of versatile loading and effective firing of nanobullets (nB), as novel tools toward advancing microscale tissue penetration of therapeutic payloads. The electrochemically synthesized hollow microcannons have been

Received: November 9, 2015
Accepted: December 21, 2015





DOI: 10.1021/acsnano.5b07080
ACS Nano XXXX, XXX, XXX−XXX

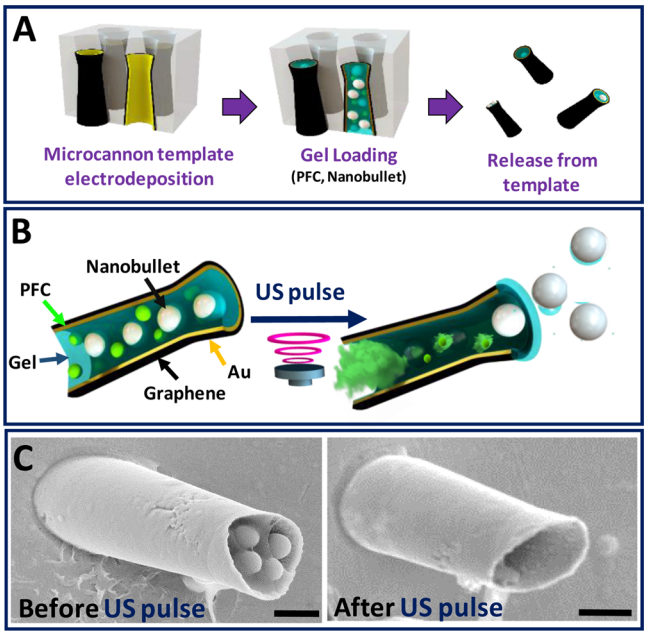


**Figure 1. Ultrasound-triggered nB firing based on vaporization of PFC droplets as a propulsion system. (A) Microcannon (Mc) fabrication by template electrodeposition, loading of cargoes by infiltrating them inside a gel matrix into the interior of the hollow Mcs and releasing the Mc from the template. (B) Mc composition (left) and schematic illustrating the firing of nanobullets (nB) from Mc by the spontaneous PFC vaporization upon application of US pulse (right). (C) SEM images (different Mc from the same batch) showing the nB-loaded Mc before (left) and after (right) the US-triggered firing. Scale bar, 20 $\mu$m.**

fully loaded with a gel matrix containing the nB and a perfluorocarbon (PFC) emulsion (Figure 1A). The ultrasound (US)-triggered vaporization of the PFC emulsion,[25,26] confined inside the Mc, results in the rapid ejection of the nB, reaching remarkable speeds (on the scale of meters per second), analogous to the firing of a bullet through a barrel of a gun (Figure 1B). The new microballistic concept was theoretically modeled and experimentally demonstrated. Deep penetration capabilities were demonstrated by firing the nB from an array of static Mc into a phantom gel target.

US-triggered vaporization of perfluorocarbon micro-emulsion is an extremely attractive candidate for externally triggering the actuation of such micro/nanoscale ballistic tools, as it is biocompatible[27,28] and has been previously used to enhance the permeation and delivery of therapeutics into blood vessels and tissue.[29−39] However, there are no reports of acoustic microcannons capable of firing nanobullets. We expect that the new US-based ballistic approach could lead to efficient delivery devices capable of delivering a wide range of payloads deep into an identified target.

## RESULTS AND DISCUSSION

A schematic of the synthesis of acoustically triggered Mcs is illustrated in Figure 1A. First, the hollowed cone structure of the Mc was fabricated using template electrodeposition of electrochemically reduced graphene oxide (erGO) and gold (Au) on the walls of micropores in a polycarbonate membrane; see experimental section and further details in Martin *et al.*[40] Afterward, a liquid gel matrix (at 40 °C), containing 1 $\mu$m silica nBs and PFC emulsions, was infiltrated by gravitational and capillarity forces into the hollow Mcs anchored in the template membrane.[41,42] After cooling down to room temperature, the particles were entrapped in the solidified gel matrix which served as a stabilizer and scaffold to protect and retain the loaded nB and PFC emulsion within the Mc interior.

A schematic of the Mc components and operation is shown in Figure 1B. Upon application of a focused ultrasound pulse by a piezoelectric transducer (see Methods and Figure S1), the nBs are ejected rapidly from the Mc. The mechanism responsible for the propulsion thrust of the nB relies on the momentum associated with the ultrasound-induced spontaneous vaporization of the PFC emulsion droplet into a rapidly expanding microbubble. The subsequent expulsion of these microbubbles from one opening of the Mc structure leads to the ejection of nBs, thereby displacing the Mc. The ejection of the nB from the Mc structure is further supported by Figure 1C and Figure S2, which shows SEM micrographs of MC before and after the US pulse. While the nBs are initially packed in the gel within the Mc, the cannon is nearly empty after the ultrasound pulse, reflecting the PFC vaporization and the ejection of the nBs.

Figure 2A and Video S1 illustrate a vaporized PFC gas bubble which is clearly visible after the US pulse. The rapid emulsion expansion during the vaporization process provides a sudden impulse that projects and displaces both Mc and nB out of the microscope field vision leaving a PFC gas cloud behind.

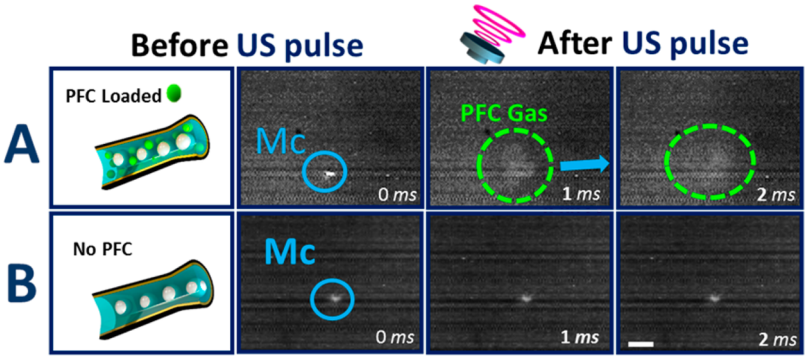


**Figure 2. Mc loading schematic and time-lapse images of the Mc before (left) and after (right) application of US pulse, taken from Video S1 at 1 ms intervals. (A) Images illustrating the US-triggered vaporization of the PFC-emulsion embedded inside the Mc. The rapid expansion of the PFC microbubble is responsible for the firing and propulsion thrust of the nB. (B) In the absence of PFC in the Mc, no firing, motion, or ejection is produced. Scale bar, 45 $\mu$m.**



DOI: 10.1021/acsnano.5b07080
*ACS Nano* XXXX, XXX, XXX−XXX

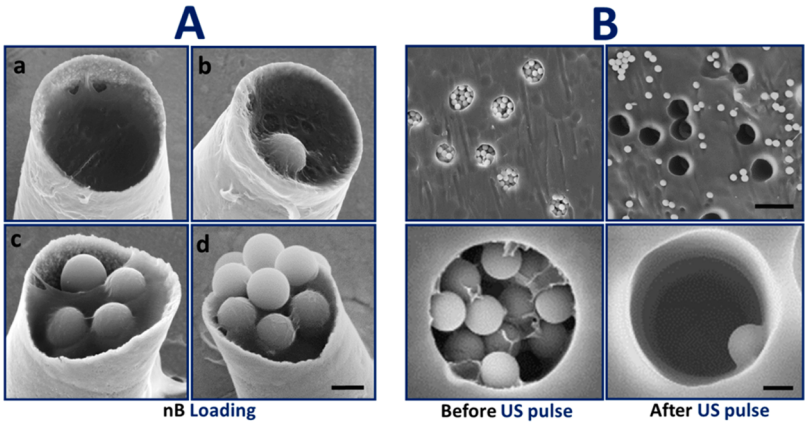


**Figure 3. (A) SEM micrographs illustrating tunable nB loading density in the gel matrix: (a) no nB, (b) low nB concentration, (c) medium nB concentration, and (d) high nB concentration (scale bar, 1 $\mu$m). (B) SEM micrographs showing firing characterization of static Mc confined within multiple micropores of the template membrane (top; scale bar, 10 $\mu$m) and detail of single Mc. (bottom; scale bar, 1 $\mu$m); before the US pulse (left) and the ejection of cargo nB after the US pulse (right).**

In our case, perfluorononane is used as the PFC fuel, and although it has a boiling point of 125−126 C°,[43] under application of an ultrasound pulse it displays a spontaneous phase shift from a liquid to a gas state.[35] Such vaporization event results from the collapse of the PFC gas microbubbles after the peak negative pressure exceeds its threshold, indicating that this process does not follow linear or exponential dependence on the applied ultrasound power. While the nB ejection from the Mc cannot be recorded from these images, such firing will be clearly documented in the following sections. Subsequent control experiments were performed using silica nB-loaded Mc structures without the PFC emulsion. No firing, motion of Mc, or ejection of bullets is observed in this case (see Video S1 and Figure 2B), supporting the hypothesis that the firing is caused by vaporization of the PFC emulsion (as was demonstrated previously by Kagan *et al.*[19]), and not by an acoustic pressure displacement.

The number of nB loaded into the Mc can be adjusted by controlling the density of the nB embedded in the gel matrix, as shown in Figure 3A. These scanning electron microscopy (SEM) micrographs demonstrate the efficient and tailored loading of different nB concentrations inside the Mc structure: from a gel matrix not containing nBs (Figure 3A,a) to a high packing density of nB (with minimal gaps) using the original commercial nB concentration (Figure 3A,d). Further (1:1000 and 1:100) dilutions of the original concentration result in low or medium nB loadings, respectively (Figure 3A,b,c).

To obtain a better characterization and visualization of the firing mechanism, we evaluated static Mcs prepared using the same template electrodeposition protocol, but without dissolving the polycarbonate template. This leads to an array of multiple confined microcannons pointing in the same direction. The SEM images of Figure 3B illustrate the loading and ejection of nBs from the static microcannons (eight Mcs on top and a single one on bottom). Each micropore of the template membrane contains a bilayer graphene/gold tubular Mc structure and is fully loaded with PFC emulsions and silica-nBs within the gel matrix. The loading mechanism of the cargo by a gel matrix is efficient, reproducible and essential to maintain the tightly packed cargo inside the cannon; free nBs outside the micropore membrane structure are removed during a thorough washing procedure (see Figure 3B left). After application of the US pulse, the silica nBs are ejected from the micropores and released toward the upper part of the membrane. A negligible number of silica bullets remain in the Mc structure (see Figure 3B right). Such ability to fire a large amount of nBs is essential for enhanced effectiveness (*e.g.*, therapeutic efficacy in drug delivery).

To further assess the distance reached by the nBs and demonstrate the versatility of the microballistic approach for loading and shooting different cargoes, static Mcs, confined in the template membrane (as in Figure 3B), were loaded with fluorospheres (Fs) that were fired toward a tissue phantom gel. The loading of the Fs nBs and the PFC was similar to the previous approach involving silica nBs (see Methods for details). The tissue phantom gel has acoustic and mechanical properties comparable to real tissues,[44] allowing for the measurement of the distance traveled by these fired nBs and the examination of the penetration capabilities of the presented microballistic approach. Figure 4 shows the corresponding fluorescence (top and cross-section) images before and after the US pulse. The top view in Figure 4A illustrates the Mcs

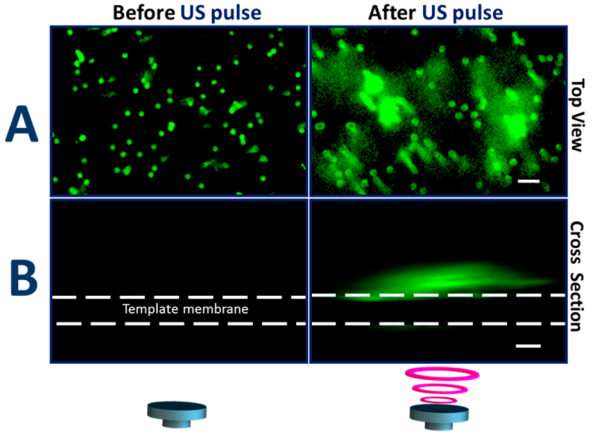


**Figure 4. Fluorescence images of fluorosphere (Fs)-loaded static Mcs confined in the template membrane (left) and the distribution of the Fs bullets after the US-triggered firing inside a tissue phantom gel matrix (right). (A) Top view, where each point represents one microcannon loaded with Fs bullets. Scale bar, 20 $\mu$m. (B) Cross section view showing the distance of the bullet penetration within the agar. Scale bar, 20 $\mu$m.**



DOI: 10.1021/acsnano.5b07080
*ACS Nano* XXXX, XXX, XXX−XXX

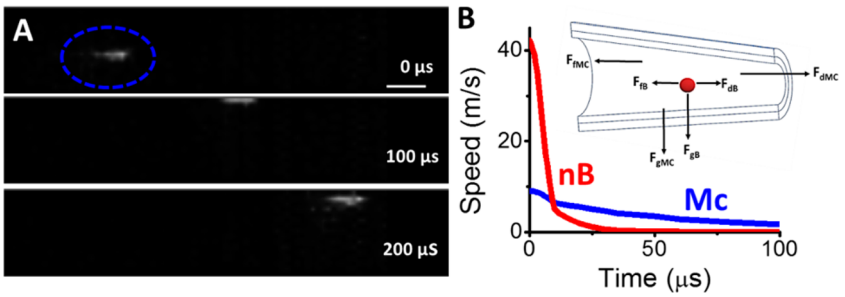


**Figure 5. Experimental and theoretical behaviors of microcannon (Mc, blue) and nanobullet (nB, red) upon firing. (A) Time-lapse frames (0–200 $\mu$s) illustrating the displacement of the Mc (circled in blue) upon application of a US pulse recorded under high frame rate (the nB ejection is not shown due to their ultrafast speed). Scale bar, 20 $\mu$m. (B) Theoretical speed profile of the Mc and nB upon firing; the inset shows schematic of the forces experienced by the Mc and nB, including force of friction ($F_f$), force of gravity ($F_g$), and drag force ($F_d$), with the latter being the dominating force.**

filled with the fluorescent particles prior to the US pulse (Figure 4A left) with each point represents a Mc. A fluorescence "cloud" is observed after the US-triggered firing (Figure 4A right), illustrating the Fs distribution on the tissue phantom and demonstrating the successful ejection of the Fs nBs from the static Mc upon application of ultrasound. The cross section view in Figure 4B shows the nBs penetrating 17.5 ± 3.7 $\mu$m into the tissue phantom after application of the ultrasound pulse.

Due to technological limitations for capturing the nB ejection from the Mc (associated with their ultrafast ejection speed and size), a theoretical model was used to predict the nB behavior. See more information in the Supporting Information. Taking into consideration that both the Mc and the nB are exposed to the same propulsion thrust of the PFC explosion, the speeds for nB could be modeled by measuring the displacement of the Mc (Figure 5A) and extrapolating the force to the nB. The Reynolds number, which estimates the relation between viscous and inertial forces,[4,9] was calculated to be 13.7 (see more information in the Supporting Information). This low Re means that the Mc moves in a laminar flow where viscous forces dominate the motion; thus, the inertia of the objects is negligible.[3,45] Figure 5B shows a scheme of the forces acting in the two objects under study, the Mc and the nB. These include the force of friction (not considered for the calculation), the gravitational force and the hydrodynamic drag force. The latter is the primary force involved in the propulsion, defined by Stokes's law, and is proportional to the speed of the object. The proportionality constant, $k$, depends on the shape of the object under study, so it differs from the Mc (cylinder) and the nB (sphere) as detailed in Table S1. Since the drag force is responsible for the movement, the instantaneous and initial speeds for an object subject to this propulsion mechanism will be defined following eqs 1 and 2, respectively, where $v$ and $v_0$ are the instantaneous and initial speeds, respectively, the interval of time in which the object displaces by $\Delta x$, and $m$ is the mass of the object. The drag factors $k$ for a cylindrical-shaped Mc and for a spherical nB[46] were calculated to be $8.8 \times 10^{-8}$ and $1.9 \times 10^{-8}$ kg·s$^{-1}$ respectively.

$$v = v_0 \, e^{-kt/m} \tag{1}$$

$$v_0 = \frac{k\Delta x}{m(1 - e^{-tk/m})} \tag{2}$$

The Mc displacement was captured using a high-speed camera by considering the change in position of the microcannon over the time considered, resulting in an average speed of 1.05 ± 0.26 m·s$^{-1}$ ($n$ = 3). Then, the initial Mc speed was estimated to be 9.0 m·s$^{-1}$, according to eq 2. This value is in agreement with other microstructures propelled by perfluorocarbon.[19] The theoretical speed of the nB and the consequent initial nB velocity were calculated to be 42.2 m·s$^{-1}$, which is around 5 times faster than the speed of the Mc. The instantaneous speed–time profile was theoretically modeled for both the Mc and the nB, as shown in Figure 5B. The nB attains faster initial speed during the initial microseconds and then rapidly slows down while the speed of the Mc decays more slowly. For simplicity, these approximations were carried out considering that the force is applied only to a single nB; future studies will focus on developing a more precise theoretical simulation accounting for the ejection of multiple nBs. Overall, these theoretical predictions are in agreement with the experimental observations of the optical, fluorescence and SEM images and indicate an ultrafast ejection of the nanobullet from the microcannon.

## CONCLUSIONS

We have demonstrated the successful ballistic operation of acoustic microcannons, which allow the efficient loading and firing of nanoscale cargoes as nanoprojectiles. Such firing of large amount nB has been modeled theoretically and demonstrated experimentally. The experimental data supports the theory that the ejection of nanobullets from the microcannon occurs due to PFC vaporization, presenting high power, fast displacement speed, and a large biologically relevant tissue penetration depth. These nanobullets could thus be used to drive drugs directly deep into diseased tissues or deliver genetic material into cell nuclei for gene therapy, thus revolutionizing drug delivery and the treatment of human diseases. The materials used for fabricating the microcannon (graphene and gold layers) are biocompatible and widely used for biomedical applications.[47–49] Future work will thus aim at developing this microbullet platform technology for delivering a wide range of therapeutic payloads (including codelivery of several drugs) and expanding the practical utility of the acoustic microcannons, for their use as single or arrays devices for transporting drug cocktails and vaccines, respectively. The shape and density of the bullet could be further studied to reduce resistance so that the nanobullets would penetrate through the target tissue without dispersing much of its energy. In addition, adding magnetic cargo would allow positioning of the microcannons while firing their load. This study thus paves


DOI: 10.1021/acsnano.5b07080
ACS Nano XXXX, XXX, XXX–XXX

the way for creating next-generation efficient nanoscale delivery devices capable of delivering their payloads into an identified target, toward the realization of the "magic bullets" vision.

## METHODS

**Perfluorononane Emulsion Preparation.** Perfluorononane (PFN) nanoemulsions purchased from Sigma-Aldrich (St. Louis) were prepared in phosphate buffer saline (PBS). A volume ratio of 3:1:1 of PBS/ anionic fluorosurfactant/PFN was prepared through probe-type sonication. The tube containing PBS was immediately placed in a heating block at 90 °C for 5 min, and 200 μL of Zonyl FSE (Sigma-Aldrich, St. Louis) anionic fluorosurfactant was added. The solution was vortexed until homogenized. A 200 μL aliquot of PFN (from Sigma-Aldrich, St. Louis) was added to the PBS-Zonyl FSE mixture. The probe of the sonicator was lowered in the tube about 8 mm from the bottom. While still in the ice bath, the sonicator was operated with a LabVIEW program interfaced with the sonicator via (a foot pedal input and a reed relay board. The program delivered three 0.5 s bursts and was repeated 60 times. The short bursts prevented the solution from stirring violently and producing foam; a 2 s delay between each set of 3 bursts served to prevent overheating. This process resulted in a 20% vol. PFN emulsion which was stable and turbid in appearance. Emulsion sizes and zeta potentials were measured by dynamic light scattering with a Zetasizer Nano-ZS (Malvern Instruments, Worcestershire, U.K.). The 20% vol PFN emulsion was diluted to 1% vol by a PBS pH 7.4 solution before incubating with the Mcs.

**Microcannon Synthesis.** The Mcs were prepared by electrochemical template synthesis of graphene and gold layers.[40] The outer layer of electrochemically reduced graphene oxide (erGO) was prepared by the electrochemical reduction of graphene oxide (GO, graphene supermarket, New York, USA) into 5 μm diameter conical pores of a polycarbonate membrane (Catalog No. 7060−2513; Whatman, Maidstone, U.K.). A thin gold film was first sputtered on the branched side of the membrane to serve as a working electrode. The membrane was assembled in a Teflon plating cell with aluminum foil serving as an electrical contact for the subsequent electrodeposition. Graphene oxide (GO, 0.1 mg $mL^{-1}$) was first dispersed in a solution containing 0.1 M $H_2SO_4$ and 0.5 M $Na_2SO_4$ purchased from Sigma-Aldrich (St. Louis) by ultrasonication for 15 min. The resultant homogeneously dispersed brown GO can be stable for several weeks because of the high presence of oxygen functionalities. The simultaneous electrochemical reduction and deposition of GO was carried out using cyclic voltammetry (CV, over +0.3 to −1.5 V vs Ag/AgCl (3 M KCl) from (CH Instrument, Austin, TX), at 50 mV $s^{-1}$, for five cycles; $n = 5$), using a Pt wire as counter electrode. Subsequently, a gold layer was plated inside the erGO layer acting as a scaffold or supporting layer for the graphene not to collapse. The gold layer was plated at −0.9 V using a charge of −1.5 C from a commercial gold plating solution (Orotemp 24 RTU RACK; Technic Inc.). The sputtered gold layer was gently removed by hand polishing with 3−4 μm alumina slurry.

Gelatin purchased in a local supermarket was prepared at 40 mg $mL^{-1}$ by dissolving in water heating at 40 °C and later cooling it to room temperature allowing it to solidify. Then 100 μL of PFN (dilution 1:100 from the synthesized), 50 μL of silica particles (1 μm Polysciences,) and 50 μL of gelatin were infiltrated in the resulting membrane and allowed to cool and dry until complete dryness and solidification of the gelatin in the pores. The surplus gelatin outside of the pores was washed thoroughly with a swab. The membrane was then dissolved in methylene chloride for 5 min to completely release the Mcs. The Mcs were collected by centrifugation at 7000 rpm for 3 min and washed repeatedly with ethanol and three times with ultrapure water (18.2 Ω cm), with a 3 min centrifugation following each wash. All Mcs were used after synthesis at room temperature. For the tailored loading of nB inside the Mc, the density of the embedded silica Nb was controlled by changing the concentration from the original commercial silica solution (MicroSil Microspheres), obtaining "high loading" at 1:1 ratio, "medium loading" at 1:100 dilution ratio, and "low loading" at 1:1000 dilution ratio.

For static Mc experiments, the same Mc synthesis and cargo loading methodology was used, but without dissolving the polycarbonate membrane template, allowing to act as an array of statics Mc. Note that for the fluorescence experiments with static Mc, the Mc were loaded by infiltrating with a solution of 50 μL of Fluorospheres microsphere solution (f8803, Invitrogen; 0.5 mg/mL), instead of the silica particles. These fluorescence experiments were performed inside a tissue phantom gel made of 0.5% weight of Agarose (Sigma-Aldrich).

**Acoustic-Microcannon Firing of Nanobullets.** Mc propulsion was initiated by exposure to a focused ultrasound pulse using a custom designed ultrasound and microscope system.[44] A PCI-5412 arbitrary waveform (National Instruments, Austin, TX) was used to create a single 10 ms long US pulse at 2.25 MHz. A 300 W amplifier (Vox Technologies, Richardson, TX) was used to create a peak negative pressure of 1.9 MPa at the focal zone with a Panametrics V305-SU transducer (Olympus NDT Inc., Waltham, MA). A custom-designed LabVIEW 8.2 program was utilized to initiate the US pulses. The transducer was submerged in a water tank while a Petri dish containing the sample was positioned at the water surface placing the sample in both the focal zone of the optics and the US transducer as previously described by Ibsen *et al.*[44] and schematically represented in Figure S1.

In order to capture the Mc propulsion, videos were acquired at 10 000 or 18 000 frames per second (fps) using a FASTCAM 1024 PCI high-speed camera (Photron, San Diego, CA) and a 20X objective. Frame rates of 45 000 and 109 500 fps were used for capturing the motion of bubbles resulting from emulsion vaporization. For static Mc experiments, the template membrane with the embedded motors was placed on a Petri dish. Experiments showing the ejection of silica nB from the Mc were performed in water in a Petri dish. The experiments showing the ejection of fluorescent Fs were performed with static Mc anchored in the flexible template membrane strips embedded at the bottom of a 0.5% agarose tissue phantom that was placed inside. After applying the ultrasound pulse, the tissue phantom was sectioned and imaged in cross section using a Nikon Eclipse 80i upright microscope with a fluorescence B2-A FAM filter to determine the distance over which the fluorescent Fs nB had penetrated into the phantom. It should be noted that there is a small agar filled gap between the template membrane and the Petri dish, generating a green fluorescent line at the bottom of the membrane after the US pulse (Figure 4B). The SEM images were taken with a Phillips XL30 ESEM instrument.

## ASSOCIATED CONTENT

### Supporting Information

The Supporting Information is available free of charge on the ACS Publications website at DOI: 10.1021/acsnano.5b07080.

Additional figures and expanded speed modeling of microcannon (PDF)

Acoustic droplet vaporization of PFC emulsions after applying an US pulse to a PFC/silica nBs-loaded Mc and control Mc without PFC emulsion (AVI)

## AUTHOR INFORMATION


### Corresponding Authors

*E-mail: sesener@ucsd.edu.

*E-mail: josephwang@ucsd.edu.

### Author Contributions

‖F.S. and A.M. contributed equally to this work.


### Notes

The authors declare no competing financial interest.

## ACKNOWLEDGMENTS

This work was supported by the Defense Threat Reduction Agency Joint Science and Technology Office for Chemical and



DOI: 10.1021/acsnano.5b07080
ACS Nano XXXX, XXX, XXX−XXX

Biological Defense (Grant Nos. HDTRA1-13-1-0002 and HDTRA1-14-1-0064). F. S. and A. M. acknowledge fellowships from the UC MEXUS-CONACYT and the Spanish Ministry of Education, Culture and Sports, respectively.

## REFERENCES

(1) Sanhai, W. R.; Sakamoto, J. H.; Canady, R.; Ferrari, M. Seven Challenges for Nanomedicine. *Nat. Nanotechnol.* **2008**, *3*, 242−244.
(2) Wang, J. *Nanomachines: Fundamentals and Applications*; Wiley-VCH: Weinheim, Germany, 2013.
(3) Purcell, E. M. Life at Low Reynolds Number. *Am. J. Phys.* **1977**, *45*, 3−11.
(4) Feynman, R. P. There's Plenty of Room at the Bottom. *Eng. Sci.* **1960**, *23*, 22−36.
(5) Walker, D.; Kübler, M.; Morozov, K. I.; Fischer, P.; Leshansky, A. M. Optimal Length of Low Reynolds Number Nanopropellers. *Nano Lett.* **2015**, *15*, 4412−4416.
(6) Zhao, G.; Nguyen, N. T.; Pumera, M. Reynolds Numbers Influence the Directionality of Self-Propelled Microjet Engines in the 10−4 Regime. *Nanoscale* **2013**, *5*, 7277.
(7) Nelson, B. J.; Kaliakatsos, I. K.; Abbott, J. J. Microrobots for Minimally Invasive Medicine. *Annu. Rev. Biomed. Eng.* **2010**, *12*, 55−85.
(8) Solovev, A. A.; Sanchez, S.; Pumera, M.; Mei, Y. F.; Schmidt, O. G. Magnetic Control of Tubular Catalytic Microbots for the Transport, Assembly, and Delivery of Micro-objects. *Adv. Funct. Mater.* **2010**, *20*, 2430−2435.
(9) Wang, W.; Duan, W.; Ahmed, S.; Mallouk, T. E.; Sen, A. Small Power: Autonomous Nano- andMmicromotors propelled by self-generated gradients. *Nano Today* **2013**, *8*, 531−554.
(10) Wang, H.; Pumera, M. Fabrication of Micro/Nanoscale Motors. *Chem. Rev.* **2015**, *115*, 8704−8735.
(11) Chałupniak, A.; Morales-Narváez, E.; Merkoçi, A. Micro and Nanomotors in Diagnostics. *Adv. Drug Delivery Rev.* **2015**, *95*, 104.
(12) Kim, K.; Guo, J.; Xu, X.; Fan, D. L. Recent Progress on Man-Made Inorganic Nanomachines. *Small* **2015**, *11*, 4037−4057.
(13) Sánchez, S.; Soler, L.; Katuri, J. Chemically Powered Micro- and Nanomotors. *Angew. Chem., Int. Ed.* **2015**, *54*, 1414−1444.
(14) Soler, L.; Magdanz, V.; Fomin, V. M.; Sanchez, S.; Schmidt, O. G. Self-Propelled Micromotors for Cleaning Polluted Water. *ACS Nano* **2013**, *7*, 9611−9620.
(15) Singh, V. V.; Soto, F.; Kaufmann, K.; Wang, J. Micromotor-Based Energy Generation. *Angew. Chem., Int. Ed.* **2015**, *54*, 6896−6899.
(16) Cheng, R.; Huang, W.; Huang, L.; Yang, B.; Mao, L.; Jin, K.; ZhuGe, Q.; Zhao, Y. Acceleration of Tissue Plasminogen Activator-Mediated Thrombolysis by Magnetically Powered Nanomotors. *ACS Nano* **2014**, *8*, 7746−7754.
(17) Gao, W.; Dong, R.; Thamphiwatana, S.; Li, J.; Gao, W.; Zhang, L.; Wang, J. Artificial Micromotors in the Mouse's Stomach: A Step Toward *in Vivo* Use of Synthetic Motors. *ACS Nano* **2015**, *9*, 117−123.
(18) Xi, W.; Solovev, A. A.; Ananth, A. N.; Gracias, D. H.; Sanchez, S.; Schmidt, O. G. Rolled-Up Magnetic Microdrillers: Towards Remotely Controlled Minimally Invasive Surgery. *Nanoscale* **2013**, *5*, 1294−1297.
(19) Kagan, D.; Benchimol, M. J.; Claussen, J. C.; Chuluun-Erdene, E.; Esener, S.; Wang, J. Acoustic Droplet Vaporization and Propulsion of Perfluorocarbon-Loaded Microbullets for Targeted Tissue Penetration and Deformation. *Angew. Chem., Int. Ed.* **2012**, *51*, 7519−7522.
(20) Wang, W.; Li, S.; Mair, L.; Ahmed, S.; Huang, T. J.; Mallouk, T. E. Acoustic Propulsion of Nanorod Motors Inside Living Cells. *Angew. Chem., Int. Ed.* **2014**, *53*, 3201−3204.
(21) Esteban-Fernandez de Ávila, B.; Martin, A.; Soto, F.; Lopez-Ramirez, M. A.; Campuzano, S.; Vasquez-Machado, G. M.; Gao, W.; Zhang, L.; Wang, J. Single Cell Real-Time miRNAs Sensing Based on Nanomotors. *ACS Nano* **2015**, *9*, 6756−6764.
(22) Gautam, U. K.; Panchakarla, L. S.; Dierre, B.; Fang, X.; Bando, Y.; Sekiguchi, T.; Govindaraj, A.; Golberg, D.; Rao, C. N. R. Solvothermal Synthesis, Cathodoluminescence, and Field-Emission Properties of Pure and N-Doped ZnO Nanobullets. *Adv. Funct. Mater.* **2009**, *19*, 131−140.
(23) Pissuwan, D.; Valenzuela, S. M.; Miller, C. M.; Cortie, M. B. A Golden Bullet? Selective Targeting of Toxoplasma gondii Tachyzoites Using Antibody-Functionalized Gold Nanorods. *Nano Lett.* **2007**, *7*, 3808−3812.
(24) Elinav, E.; Peer, D. Harnessing Nanomedicine for Mucosal Theranostics—A Silver Bullet at Last? *ACS Nano* **2013**, *7*, 2883−2890.
(25) Giesecke, T.; Hynynen, K. Ultrasound-Mediated Cavitation Thresholds of Liquid Perfluorocarbon Droplets. *In Vitro Ultrasound Med. Biol.* **2003**, *29*, 1359−1365.
(26) Reznik, N.; Shpak, O.; Gelderblom, E. C.; Williams, R.; de Jong, N.; Versluis, M.; Burns, P. N. The Efficiency and Stability of Bubble Formation by Acoustic Vaporization of Submicron Perfluorocarbon Droplets. *Ultrasonics* **2013**, *53*, 1368−1376.
(27) Litvak, E.; Foster, K. R.; Repacholi, M. H. Health and Safety Implications of Exposure to Electromagnetic Fields in the Frequency Range 300 Hz to 10 MHz. *Bioelectromagnetics* **2002**, *23*, 68−82.
(28) Zanelli, C. I.; De Marta, S.; Hennige, C. W.; Kadri, M. M. Beamforming for Therapy with High Intensity Focused Ultrasound (HIFU) Using Quantitative Schlieren. *IEEE Ultrasonics Symposium* **1993**, 1233−1238.
(29) Ibsen, S.; Benchimol, M.; Simberg, D.; Schutt, C.; Steiner, J.; Esener, S. A Novel Nested Liposome Drug Delivery Vehicle Capable of Ultrasound Triggered Release of its Payload. *J. Controlled Release* **2011**, *155*, 358−366.
(30) Rosenthal, I.; Sostaric, J. Z.; Riesz, P. Sonodynamic Therapy- a Review of the Synergistic Effects of Drugs and Ultrasound. *Ultrason. Sonochem.* **2004**, *11*, 349−363.
(31) Tachibana, K.; Feril, L. B., Jr; Ikeda-Dantsuji, Y. Sonodynamic Therapy. *Ultrasonics* **2008**, *48*, 253−259.
(32) Okada, K.; Kudo, N.; Niwa, K.; Yamamoto, K. A Basic Study on Sonoporation with Microbubbles Exposed to Pulsed Ultrasound. *J. Med. Ultrasonics.* **2005**, *32*, 3−11.
(33) Zarnitsyn, V.; Rostad, C. A.; Prausnitz, M. R. Modeling Transmembrane Transport through Cell Membrane Wounds Created by Acoustic Caviation. *Biophys. J.* **2008**, *95*, 4124−4138.
(34) Skyba, D. M.; Price, R. J.; Linka, A. Z.; Skalak, T. C.; Kaul, S. Direct *In Vivo* Visualization of Intravascular Destruction of Microbubbles by Ultrasound and its Local Effects on Tissue. *Circulation* **1998**, *98*, 290−293.
(35) Ibsen, S.; Schutt, C. E.; Esener, S. Microbubble-Mediated Ultrasound Therapy: a Review of its Potential in Cancer treatment. *Drug Des., Dev. Ther.* **2013**, *7*, 375−388.
(36) Duncanson, W. J.; Arriaga, L. R.; Ung, W. L.; Kopechek, J. A.; Porter, T. M.; Weitz, D. A. Microfluidic Fabrication of Perfluorohexane-Shelled Double Emulsions for Controlled Loading and Acoustic-Triggered Release of Hydrophilic Agents. *Langmuir* **2014**, *30*, 13765−13770.
(37) Lentacker, I.; De Smedt, S. C.; Sanders, N. N. Drug Loaded Microbubble Design for Ultrasound Triggered Delivery. *Soft Matter* **2009**, *5*, 2161−2170.
(38) Wang, C.; Kang, S.; Lee, Y.; Luo, Y.; Huang, Y.; Yeh, C. Aptamer-Conjugated and Drug-Loaded Acoustic Droplets for Ultrasound Theranosis. *Biomaterials* **2012**, *33*, 1939−1947.
(39) Huang, H.; Liu, H.; Hsu, P.; Chiang, C.; Tsai, C.; Chi, H.; Chen, S.; Chen, Y. A Multitheragnostic Nanobubble System to Induce Blood-Brain Barrier Disruption with Magnetically Guided Focused Ultrasound. *Adv. Mater.* **2015**, *27*, 655−661.
(40) Martin, A.; Jurado-Sánchez, B.; Escarpa, A.; Wang, J. Template Electrosynthesis of High-Performance Graphene Microengines. *Small* **2015**, *11*, 3568−3574.
(41) Wu, Z.; Lin, X.; Zou, X.; Sun, J.; He, Q. Biodegradable Protein-Based Rockets for Drug Transportation and Light-Triggered Release. *ACS Appl. Mater. Interfaces* **2015**, *7*, 250−255.



DOI: 10.1021/acsnano.5b07080
*ACS Nano* XXXX, XXX, XXX−XXX

(42) Daglar, B.; Demirel, G. B.; Khudiyev, T.; Dogan, T.; Tobail, O.; Altuntas, S.; Buyukserin, F.; Bayindir, M. Anemone-Like Nanostructures for Non-Lithographic, Reproducible, Large-Srea, and Ultra-Sensitive SERS Substrates. *Nanoscale* **2014**, *6*, 12710−12717.
(43) Lugert, E. C.; Lodge, T. P.; Bühlmann, P. Plasticization of Amorphous Perfluoropolymers. *J. Polym. Sci., Part B: Polym. Phys.* **2008**, *46*, 516−525.
(44) Ibsen, S.; Benchimol, M.; Esener, S. Fluorescent Microscope System to Monitor Real-Time Interactions Between Focused Ultrasound, Echogenic Drug Delivery Vehicles, and Live Cell membranes. *Ultrasonics* **2013**, *53*, 178−184.
(45) Gibbs, J. G.; Zhao, Y. Design and Characterization of Rotational Multicomponent Catalytic Nanomotors. *Small* **2009**, *5*, 2304−2308.
(46) Li, L.; Wang, J.; Li, T.; Song, W.; Zhang, G. Hydrodynamics and Propulsion Mechanism of Self-Propelled Catalytic Micromotors: Model and Experiment. *Soft Matter* **2014**, *10*, 7511−7518.
(47) Bussy, C.; Ali-Boucetta, H.; Kostarelos, K. Safety Considerations for Graphene: Lessons Learnt From Carbon Nanotubes. *Acc. Chem. Res.* **2013**, *46*, 692−701.
(48) Bianco, A. Graphene: Safe or Toxic? The Two Faces of the Medal. *Angew. Chem., Int. Ed.* **2013**, *52*, 4986−4997.
(49) Li, N.; Zhao, P.; Astruc, D. Anisotropic Gold Nanoparticles: Synthesis, Properties, Applications, and Toxicity. *Angew. Chem., Int. Ed.* **2014**, *53*, 1756−1789.


DOI: 10.1021/acsnano.5b07080
*ACS Nano* XXXX, XXX, XXX−XXX